sustainability

MDPI

Article

Energy Distribution and Working Characteristics of PIPVT Dual-Energy Module

Bochao Zhou [1], Hailong Li [1], Chao Wang [1], Di Wang [2] and Xiaoyan Ma [3,*]

[1] College of Metropolitan Transportation, Beijing University of Technology, Beijing 100124, China; bczhou@bjut.edu.cn (B.Z.); lihailong@emails.bjut.edu.cn (H.L.); wangchao@bjut.edu.cn (C.W.)
[2] Department of Civil Engineering, University of Ottawa, Ottawa, ON K1N 6N5, Canada; dwang6@uottawa.ca
[3] School of Materials Science and Engineering, Chang'an University, Xi'an 710064, China
* Correspondence: xiaoyanma@chd.edu.cn

Abstract: The pavement integrated photovoltaic/thermal (PIPVT) system can comprehensively use solar energy to generate electricity and heat, which is an effective way to use new energy. In this study, we couple heat conduction and convection from the Optics, Electrics, and Solids Modules in the COMSOL Multiphysics Module to build a PIPVT element model to fully understand the energy distribution within the dual-energy module. The simulation results show that when circulating water is introduced into the photovoltaic panels, the temperature on the back of the photovoltaic panels is reduced by 30 °C, and the temperature of the entire dual-energy module board is reduced by 10–15 °C. The introduction of a thermal collector module (T module) can effectively dissipate heat to extend the life of PV modules, and also improve their work efficiency. PIPVT's solar energy utilization rate is 39.4%, which is a significant improvement compared to the 14.3% solar energy utilization rate of the photovoltaic module (PV module) alone and the 18.7% solar energy utilization rate of the T module. It shows that the dual-energy module has a synergistic effect.

Keywords: solar energy; PIPVT; COMSOL Multiphysics 6.0; dual-energy module; energy distribution

Citation: Zhou, B.; Li, H.; Wang, C.; Wang, D.; Ma, X. Energy Distribution and Working Characteristics of PIPVT Dual-Energy Module. *Sustainability* **2024**, *16*, 9151. https://doi.org/10.3390/su16219151

Received: 20 July 2024
Revised: 18 October 2024
Accepted: 20 October 2024
Published: 22 October 2024

1. Introduction

The burning of traditional fossil fuels has exacerbated global warming, so finding a sustainable and clean energy alternative to traditional fuels can effectively reduce carbon dioxide emissions [1]. This may be one of the important reasons why solar energy is widely used as a sustainable energy source. Solar photovoltaic power generation does not lead to the emission of greenhouse gases and other harmful waste gases, which has a positive impact on the environment. As an emerging clean energy source, it does not rely on traditional energy supplies, thus avoiding energy shortages [2]. So, it is the highest-potential clean energy source [3]. Between 2006 and 2018, the capacity of solar photovoltaic (PV) increased from 6.6 GW to more than 500 GW [4], which shows the rapid development of solar PV technology. At present, the main application areas of photovoltaic power generation technology are power stations in various environments [5], building walls [6] and their roofs [7], and parking lots [8]. In the field of roads, photovoltaic sound screens [9], photovoltaic road slopes [10], and photovoltaic parking sheds [11] have also been developed to a certain extent. As an important part of the photovoltaic road field, photovoltaic pavement has begun to attract more people's attention. Photovoltaic pavement technology essentially reuses wasted solar energy resources within the pavement area, without the need for additional area and resource occupation [12]. Therefore, despite the late start of photovoltaic pavement technology in road engineering, it still shows strong application potential.

One of the challenges is the efficiency of photovoltaic cells [13,14]. Only part of the solar radiation energy can be converted into electricity by photovoltaic cells; the rest is converted into heat, causing the battery temperature to rise and reducing its performance [15,16]. Therefore, solving the heat dissipation problem of photovoltaic cells can

effectively improve the power generation efficiency of photovoltaic pavement. In order to overcome the above shortcomings, drawing on the research of photovoltaic/thermal integrated buildings, the heat collector pavement can be combined with the photovoltaic pavement. Heat collector pavements typically consist of pipes embedded in the pavement structure and fluids circulating through the pipes. The pavement temperature increases as it takes in sunlight, transferring heat to the fluid in the pipe, which in turn reduces the pavement temperature because of the temperature difference [17,18]. Research findings suggest that precise temperature control of asphalt pavement during the laying process can effectively minimize top-down cracking, rutting, and other forms of distress. This plays a vital role in extending the lifespan of the pavement and reducing the need for maintenance and repairs [19–21]. Nasir et al. also proved that heat collection on the pavement is one of the measures able to alleviate the urban heat island effect through numerical simulation [22]. The heat pipe efficiently removes and collects heat generated by the photovoltaic cell's operation. This process cools the battery, enhancing power generation efficiency and solar energy utilization, while extending the road's service life.

Since the introduction of PV/T technology in 1970 [23], building integrated photovoltaic thermal hybrid (BIPVT) systems have been widely utilized on building facades or roofs [24–27]. This paper introduces the concept of applying PV and T modules to the road, expanding the application of PIPVT modules beyond the construction field, and offering a new approach for dissipating heat from photovoltaic roads. The new PIPVT module combines the advantages of both PV and T modules. PIPVT is an innovative solar energy utilization technology that combines photovoltaic power generation (PV) and thermal energy harvesting (T) systems to improve energy efficiency and extend the service life of photovoltaic cells [28]. By integrating a special photovoltaic thermal energy module into the road pavement, the PIPVT system is able to generate both electricity and heat, which can be used for building heating, hot water supply, and even snow melting and ice melting, reducing the urban heat island effect. The core components of the PIPVT system include photovoltaic cells and fluid piping. Photovoltaic cells are responsible for converting solar energy into electricity, while fluid ducts are responsible for transferring the heat generated by photovoltaic cells. This system works best in sunny weather, but performance decreases on cloudy days. The energy efficiency of the PIPVT dual-energy module far exceeds the power generation efficiency of the solar module alone [29,30]. We sought to understand the energy distribution of electrical and thermal energy in the PIPVT dual-energy module and to clarify the working characteristics of its thermal and photovoltaic parts. To achieve this, we created a PIPVT element model through multiphysics simulation. We conducted parameter setting, meshing, and physics setting, and coupled the heat conduction and thermal convection in the Optics Module, Electricity Module, and Solid Module using the COMSOL Multiphysics Module. We then plotted energy distribution curves for the independent PV module, T module, and the dual-energy module in order to reveal the working characteristics of these modules.

2. Establishment of the Model

COMSOL Multiphysics provides the ability to simulate a single physics model, as well as the flexibility to couple multiple physics models, allowing engineers and scientists to accurately analyze equipment and processes in a variety of engineering domains. The built-in model builder includes a complete modeling workflow that enables all simulation steps, from geometry modeling, material parameters, and physics settings, to solution and results processing. Compared to traditional experimental or prototype testing methods, COMSOL combines simulation analysis with experimental testing to optimize model design faster and more accurately. In addition, its built-in accurate multiphysics models can be used to test and analyze a variety of possible operating conditions and physical effects, which can help to better understand, optimize, and predict real-world engineering problems.

2.1. Geometric Modeling

Energy conversion in photovoltaic cells consists of two basic steps, i.e., photovoltaic cells absorb light to produce electron–hole pairs, which then flow electrons to the negative electrode, and holes to the positive electrode, thus producing electrical energy. The absorption spectrum range of photovoltaic cells is mainly determined by the properties, thickness, and surface characteristics of the battery materials. Since only photons with energies higher than the bandgap width of the semiconductor material can be absorbed, the bandgap of the semiconductor material determines the minimum energy (hv) of the photon that the material can absorb, i.e., the maximum wavelength. The general bandgap width is between 1 and 1.7 eV. In the solar spectrum, different wavelengths of light have different energies and different numbers of photons. As a result, the number of photons produced by the solar cells receiving light varies from one to the other. In general, crystalline silicon solar cells do not respond to infrared light with a wavelength greater than about 1200 nm and ultraviolet light with a wavelength less than about 350 nm, with a peak response of around 900 nm. Spectral response (SR) is an important index used to evaluate the conversion efficiency of solar cells. Its physical meaning is the ability of a solar cell to receive the number of amperes of current that can be produced by one watt of solar energy. Therefore, when designing a photovoltaic system, it is necessary to select the type of photovoltaic cell that is more suitable for the local spectral range according to the different spectral distributions in different regions.

Currently, two main types of photovoltaic pavement unit structures are commonly used in the industry. The first type is the grid unit structure and the second type is the hollow unit structure. In this study, a hollow structure was adopted, and the whole PIPVT module included tempered glass panels, photovoltaic cells, serpentine copper pipes, and ABS plastic bases. As shown in Figure 1, the dimensions of tempered glass and ABS plastic bases were 60 cm long × 60 cm wide, and the thickness was 2 cm and 6 cm, respectively. The solar cells were made of bendable monocrystalline high-efficiency ultra-thin flexible thin-film solar cells, which were fixed around the top edge of the ABS base using thermally conductive adhesive. The dimensions of the photovoltaic panels were 40 cm long × 40 cm wide × 2.5 mm thick, and they consisted of 36 monocrystalline silicon solar cells (125 mm × 19 mm) with a mass of only 500 g. The relevant parameters of the product include the following: maximum output power of 30 W, optimal operating voltage of 18 V, optimal operating current of 1.66 A, open circuit voltage of 20 V, short-circuit current of 1.71 A, nominal operating temperature of 45 °C (±2 °C), current temperature coefficient of ±0.05%/°C, voltage temperature coefficient of −0.33%°C, and module power temperature coefficient of −0.23%°C. This module integrates diverse physics concepts, embracing radiation interactions, radiation processes that involve various media, the transfer of heat within solid structures, the examination of laminar flow dynamics, and the movement of fluids contained within shells.

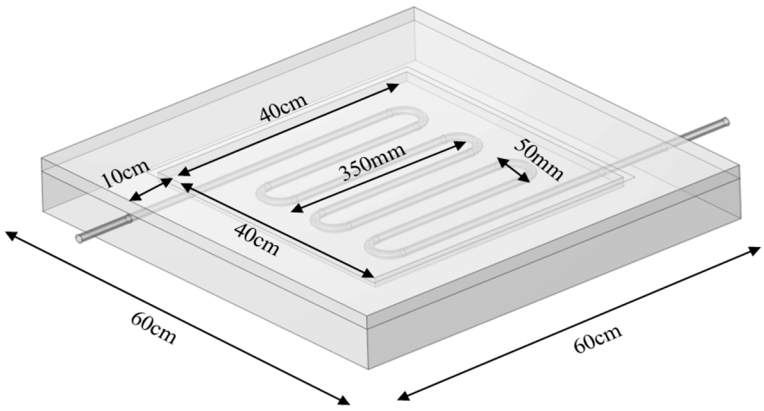

Figure 1. Model diagram of PIPVT unit structure.

During meshing, the entire cell structure is divided into different grid cell sizes, as shown in Figure 2. In order to improve the accuracy of the calculation results and shorten the calculation time, a coarse grid was adopted for the tempered glass layer and the ABS plastic base layer, and a more refined grid was adopted for the whole serpentine pipe and the connection between the serpentine pipe and the ABS base. The entire model was evenly divided using a free quadrilateral grid, and the cell dimensions were finely tuned to ensure that the maximum element size was 50 mm and the minimum element size was 5 mm. In particular, for the serpentine pipe area, the element size was further refined by scanning meshing technology with 5 elements, setting a maximum element size of 42.9 mm and a minimum element size of 3.12 mm. In addition, in order to control the uniformity of the mesh, a maximum cell growth rate of 1.4 and a curvature factor of 0.4 were set. Since the pipeline involves the study of fluids, it was necessary to set up a boundary layer; the number of layers of the boundary layer was 3, the tensile factor was 1.2, and the thickness adjustment factor was 1. The entire complete mesh contained 47,375 domain elements, 11,337 boundary elements, and 1847 edge elements.

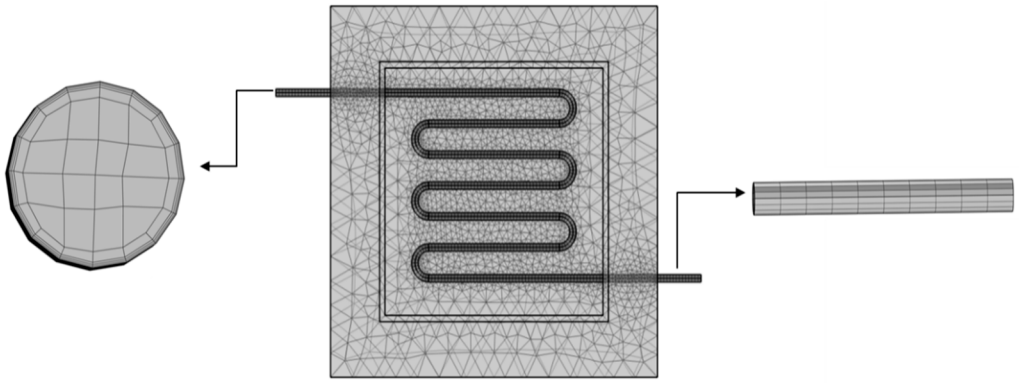

Figure 2. PIPVT cell meshing diagram.

2.2. Parameter Settings

In this paper, tempered glass panels, photovoltaic films, serpentine copper tubes, and ABS plastic bases were added from the COMSOL Material Library, with the following material parameters. In the construction of the PIPVT element model, the material parameters used in each structural layer were as follows: the thermal conductivity of the tempered glass was 1.09 W/(m·K), the density was 2500 kg/m^3, the specific heat capacity was 858 J/(kg·K), the refractive index was 1.49, the thermal conductivity of photovoltaic cells was 150 W/(m·K), the density was 2330 kg/m^3, the specific heat capacity was 700 J/(kg·K), and the conductivity was 10,000 S/m. The thermal conductivity of the ABS plastic base was 0.25 W/(m·K), the density was 1380 kg/m^3, and the specific heat capacity was 1470 J/(kg·K). The thermal conductivity of the serpentine copper tube was 400 W/(m·K), the density was 8900 kg/m^3, and the specific heat capacity was 390 J/(kg·K) [31,32].

3. Energy Distribution of PIPVT Dual-Energy Module

The PIPVT module includes surface-to-surface radiation, radiation in participating media, heat transfer in solids, laminar flow, and currents in shells. During the simulation, the following assumptions were made based on the actual situation and the characteristics of the components:

1. The accumulation of dust on tempered glass has a minimal impact on solar radiation;
2. The fluid in the serpentine pipe is evenly distributed;
3. The thermophysical properties of the fluid are constant;
4. Thermodynamic equilibrium exists between the solid phase and the fluid;

5. The thermophysical properties of the serpentine copper tube do not change with the change in temperature;
6. The heat dissipation rate on the surface and back of the PV panel is consistent.

The first computational step involves coupling three physical phenomena: surface radiation, media-involved radiation, and solid-state heat transfer. This is done to model surface radiative heat exchange and radiant heat transfer in media, and the research content is the generation and change of heat energy irradiated by sunlight on the surface of the tempered glass and sunlight irradiated into the tempered glass. Taking the coupling results of the two multiphysics fields as the initial value of the electric energy, the current physics in the shell is coupled to form a multiphysics field of electromagnetic heat, and the current and voltage value probes are set to obtain the current and voltage values at each time. Based on the coupling results of the above three multiphysics phenomena, the laminar flow is coupled into the entire multiphysics model to obtain the temperature of the fluid in the pipeline.

3.1. Solar Energy Distribution

Figure 3 shows the light intensity setting diagram of the tempered glass surface before the simulation starts. In this section, because it does not involve changing the lighting parameters, the value of the light intensity is constant at 800 W/m^2, and the light intensity distribution of the whole tempered glass surface is relatively uniform.

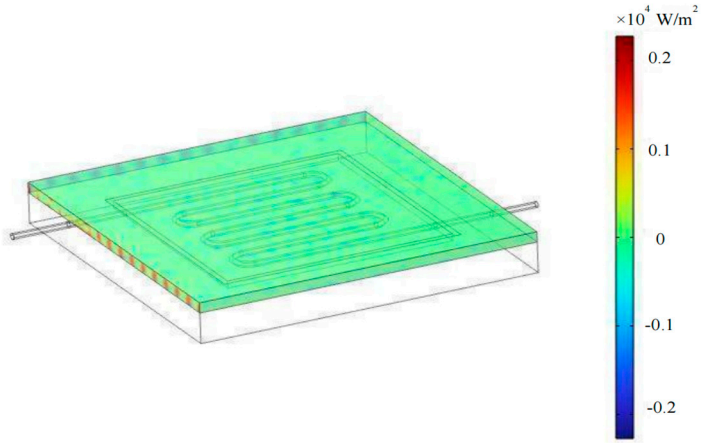

Figure 3. Light intensity setting diagram.

Figure 4 shows the surface radiant exitance of a tempered glass surface. Surface radiant exitance is a unit of measurement in which radiant power "leaves" a surface through radiation, reflection, and transmission. Before entering the circulating water, because the intensity of solar radiation is mainly concentrated in the center of the tempered glass, the area closer to the middle part absorbs a greater amount of radiation, and the surface irradiance presents a high level in the middle and a low level in the surroundings. After entering the circulating water, the distribution of the surface radiant exitance changes; the surface radiant exitance at the inlet position of the circulating water is lower than that of other positions. The size of the surface radiant exitance is related to the temperature of the material. Due to the continuous circulation of circulating water, the temperature of the whole tempered glass drops, resulting in the decrease in surface radiant exitance.

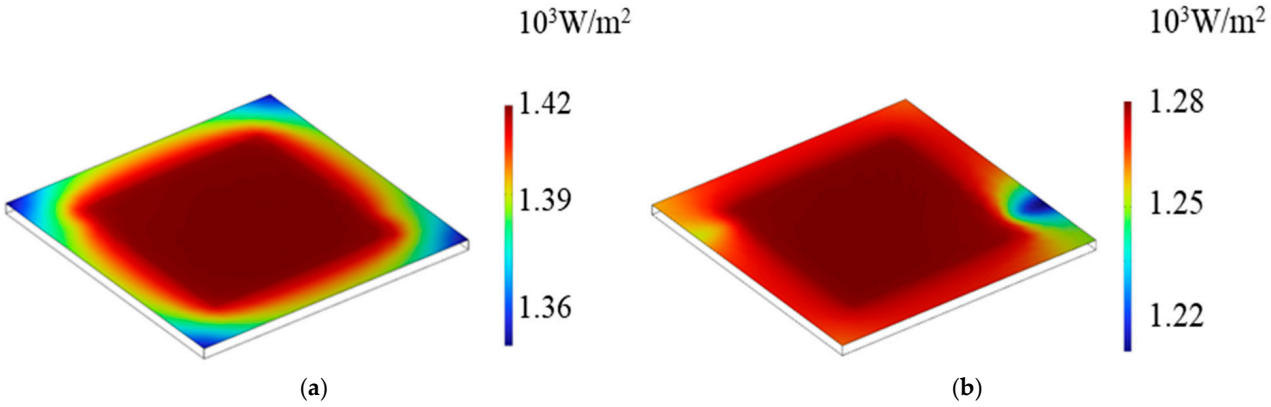

Figure 4. Radiant exitance of tempered glass surface: (**a**) before the introduction of circulating water; (**b**) after the introduction of circulating water.

3.2. Electrical Energy Distribution

In order to facilitate the calculation, the connection part of the circuit was set on both sides of the panel, and the distribution of electric potential was also higher on one side than the other, in a stepped shape. When the solar cell is running stably, the voltage value is about 19 V, and the current for stable operation is about 1.5 A according to the global calculation of COMSOL. The difference between the simulated value and the optimal operating voltage (18 V) and optimal operating current (1.66 A) of the real solar panel is small, and the results are as expected.

3.3. Thermal Energy Distribution

Figure 5 shows the heat distribution of the whole module, before the circulating water is introduced; even the minimum temperature of the ABS plastic bottom plate without solar radiation is 75 °C, and that of the tempered glass surface is close to 80 °C.

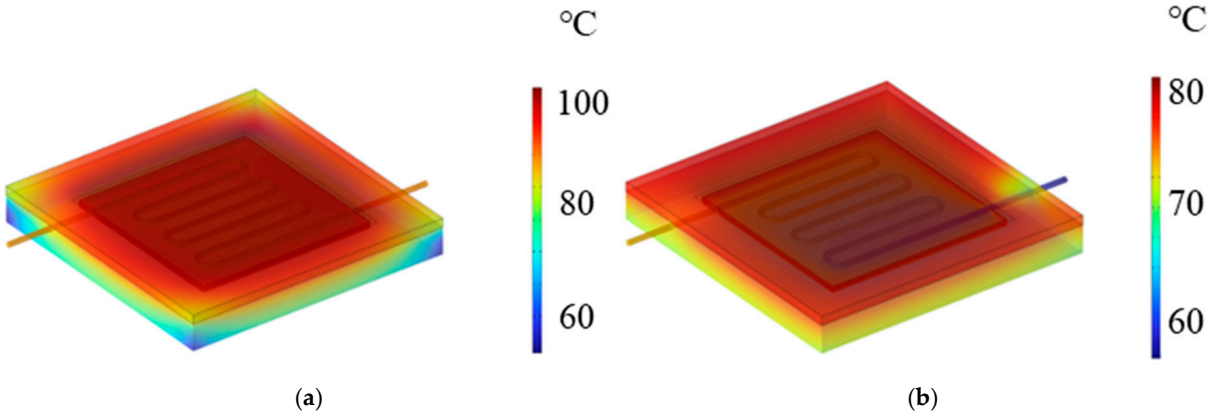

Figure 5. Temperature distribution of the overall module: (**a**) before the introduction of circulating water; (**b**) after the introduction of circulating water.

In Figure 6, the temperature distribution of circulating water on the back of the PV panel is depicted. From Figure 6a, it is evident that the temperature in the middle is higher than the ambient temperature prior to the introduction of circulating water, and the maximum temperature has reached about 100 °C, which is much higher than the normal operating battery temperature (45 °C ± 2 °C). If the photovoltaic panel is always in a state of abnormally high operating temperature, it is not conducive to long-term use. Therefore, the heat dissipation problem of photovoltaic panels needs to be solved. After the introduction of circulating water, it can be seen from Figure 6b that the temperature of the back of the photovoltaic panel decreases significantly, and the maximum temperature

decreases from 100 °C to 70 °C. It is proved that the introduction of heat pipes has a significant heat dissipation effect on photovoltaic panels. Because the photovoltaic panel is between the tempered glass and the ABS plastic bottom plate, it is not in direct contact with the vehicle in actual use, and the vehicle load has no great impact on its life. The main influencing factor is temperature. Although PIPVT cannot set the photovoltaic panel to the ideal working temperature, compared with the 100 °C of the ordinary photovoltaic pavement, it still results in a significant drop, which improves the life of the photovoltaic panel. After the circulating water is introduced, the lowest temperature is that of the pipe inlet. The temperature of the whole module is reduced by about 10–15 °C compared with before, that of the ABS plastic bottom plate is reduced to below 60 °C, and the overall heat dissipation performance has been greatly improved. Temperature has a significant impact on the power generation efficiency of photovoltaic cells. Specifically, photovoltaic cells are able to produce higher voltages at lower temperatures, so they will have higher output power in cold environments. However, when the temperature increases, the photoelectric conversion efficiency decreases because the high temperature causes the recombination rate of electrons with holes to increase, which reduces the output current of the of photovoltaic cells. In addition, before the circulating water is introduced, the temperature distribution of photovoltaic cells is high in the middle and low on all sides, and the temperature has reached close to 80 °C, which is much higher than the normal operating temperature of the battery (45 °C). If the battery is in an abnormal operating temperature state, it is not conducive to long-term use. After circulating water was introduced, the temperature of the solar panels decreased by 15 °C. The temperature of the circulating water was more noticeable in the area where it circulated, resulting in a lower overall temperature of the solar panel, which was consistent with the expected results.

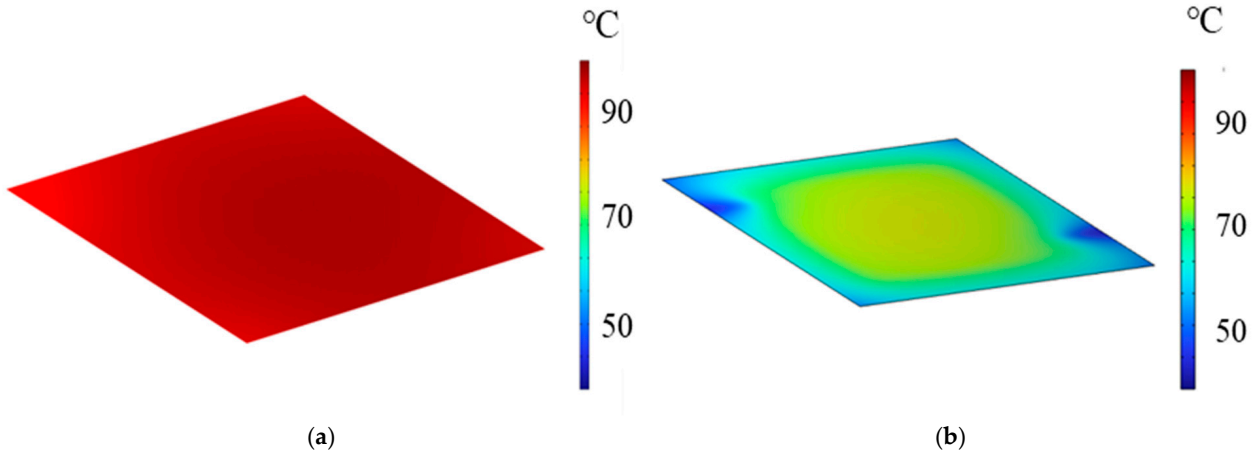

Figure 6. Temperature distribution of photovoltaic cells: (**a**) before the introduction of circulating water; (**b**) after the introduction of circulating water.

Figure 7 clearly illustrates the temperature distribution of the serpentine copper pipe. As the circulating water is pumped, the temperature of the water flow systematically increases, reaching its highest point at the outlet. Notably, there is a 12 °C temperature difference between the inlet and outlet. This echoes the result of the temperature drop of the photovoltaic cell, which reflects the heat collection effect of the PIPVT module and proves the important role of the heat collection module.

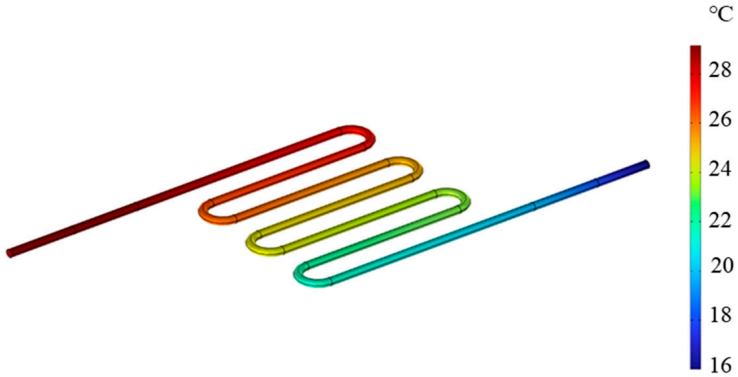

Figure 7. Temperature distribution of serpentine copper tube.

3.4. PIPVT Dual-Energy Module Independent and Cooperative Work Characteristics

In this subsection, the geometric model of the independent PV module, the independent T module, and the PIPVT dual-energy module is established, as shown in Figure 8, in which the independent PV module has no heat pipe, the ABS base part has no heat pipe holes, the independent T module part has no photovoltaic panels, the ABS base part does not have the groove under the photovoltaic panels, and the properties of the other materials are consistent with those of the PIPVT dual-energy module.

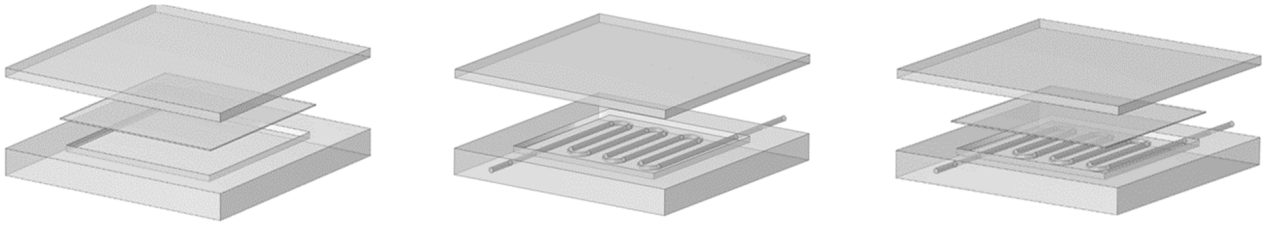

(**a**) (**b**) (**c**)

Figure 8. Geometric modeling diagram of each module: (**a**) stand-alone PV module; (**b**) stand-alone T module; (**c**) PIPVT dual-energy module.

In order to explore the independent cooperative working characteristics of the PIPVT dual-energy module, the energy values of the independent PV module, the independent T module, and the PIPVT dual-energy module were simulated and calculated, and the corresponding energy distribution maps were drawn. The different color blocks in each graph correspond to the cumulative value of different loss items, and the sum of the areas shown in the graph is the total radiation received on that day. At any given moment, the specific distribution of incident energy is represented by the length of the line segments intercepted by different color patches at that time.

3.4.1. Working Characteristics of Stand-Alone PV Module

Figure 9 shows the energy distribution of the PV module at different times of the day. The energy of the independent PV module mainly includes ambient thermal energy, PV module thermal energy, photovoltaic panel thermal energy, photovoltaic panel electrical energy, and some energy loss between various components.

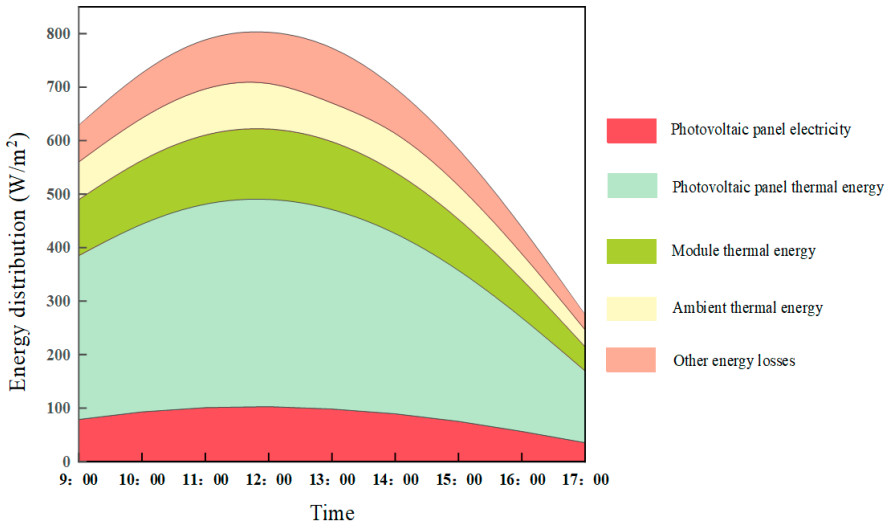

Figure 9. Energy distribution of independent PV module.

In addition to a part of the incident energy (14.3%) being converted into electrical energy output, most of the remaining energy is converted into thermal energy from the PV module and photovoltaic panels, causing the temperature of the PV module to rise, and another 17.2% is reflected into the surrounding environment by the solar cells themselves or the connections of the PV module, becoming ambient thermal energy. The other 6.7% is due to some other energy losses, such as the loss of parallel resistance in the circuit and the current loss due to non-radiative recombination. This indicates that a significant amount of the energy from the independent PV module is mainly converted into heat energy, which cannot be utilized by a standard PV module. Only a small portion of the incoming energy is able to be transformed into electrical energy. In addition, most of the heat energy in the PV module is concentrated in photovoltaic panels, which further increases the life consumption of photovoltaic cells.

3.4.2. Working Characteristics of the Independent T Module

Figure 10 shows the energy distribution of the T module at different times throughout the day, and the energy of the independent T module mainly includes ambient thermal energy, thermal T module thermal energy, photovoltaic panel thermal energy, heat pipe thermal energy, water flow thermal energy, and some energy losses between each module. Since no incident energy is converted into electrical output in the stand-alone T module, more than 90% of the energy is present in the entire system in the form of various thermal energy. Due to the lack of photovoltaic panels to generate heat energy from the thermal collection module, the thermal energy is reduced compared with the independent PV module, accounting for 42.4% of the overall energy. According to the data, the heat pipe contributes 31.4% of the total energy, while the heat energy from water flow accounts for 18.7%. The ambient temperature is 20.8% higher than that of independent PV modules, which is due to the heat pipes and water flow taking away part of the thermal energy of the PV modules, while some of the heat pipes in the model are exposed outside the PV modules. This part of the heat energy will be dissipated into the environment, and the energy loss is lower than that of independent PV modules, which is 5.4%.

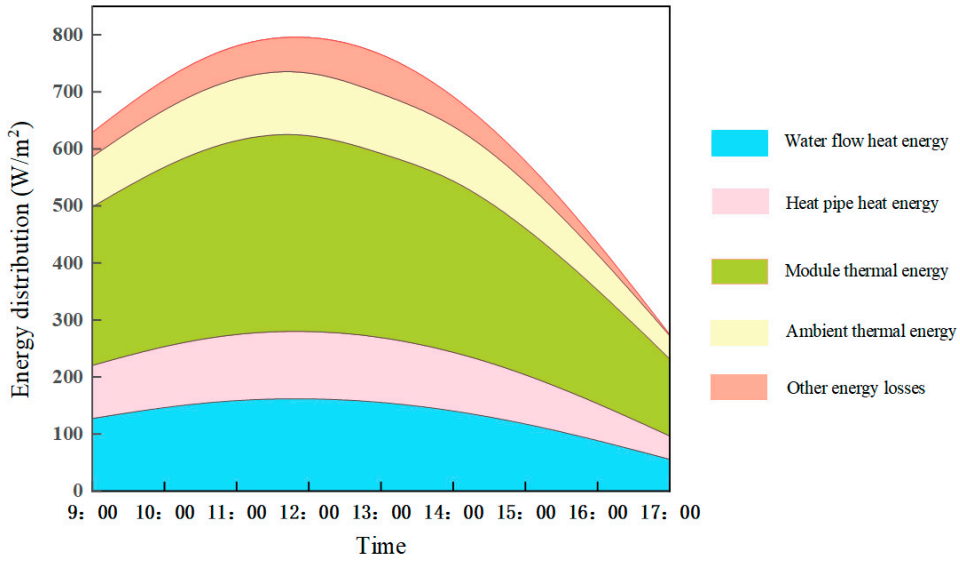

Figure 10. Energy distribution of independent heat collection modules.

3.4.3. Working Characteristics of Dual-Energy Modules

Figure 11 shows the energy distribution of the PV module at different times of the day, and the energy of the dual-energy module mainly includes ambient thermal energy, dual-energy module thermal energy, photovoltaic panel electrical energy, photovoltaic panel thermal energy, heat pipe thermal energy, water flow thermal energy, and some energy losses between the modules.

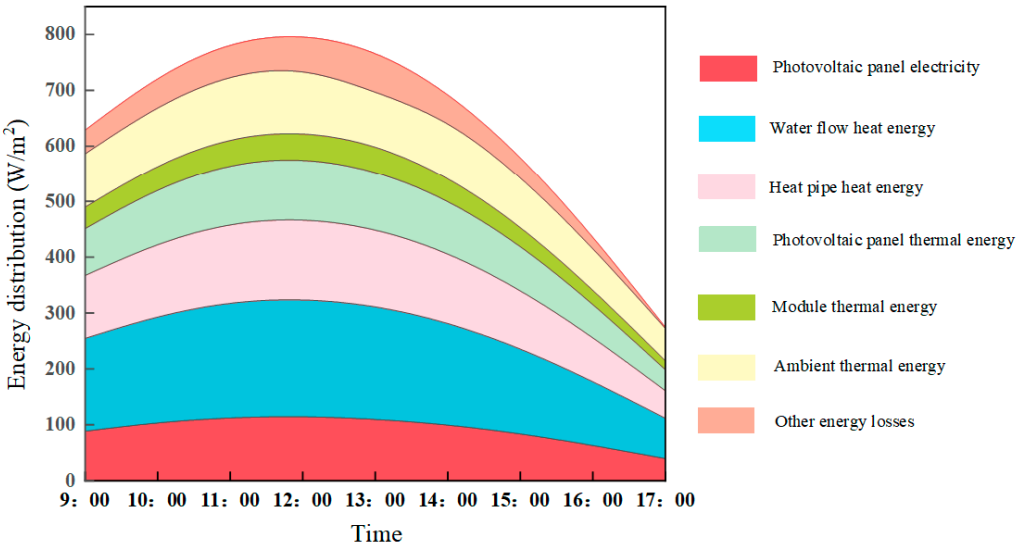

Figure 11. Energy distribution diagram of dual-energy module.

In the dual-energy module, 17.8% of the incident energy is converted into electrical energy output, which is 3.4% higher than that of the independent PV module, and only 36.6% of the remaining energy is converted into the thermal energy of the PV module, photovoltaic panel, and heat pipe that cannot be used. The unusable energy is significantly lower than that of the two independent modules, and the heat energy of the water flow increases to 21.6%. The remaining 18.9% is reflected into the surrounding environment by the solar cell itself or the connection of the PV module to become ambient thermal energy. There is also 5.1% for some other energy loss. The energy distribution of independent PV modules (just for harvesting electricity)/T modules (just for harvesting thermal energy)/PV/T modules (both for harvesting electricity and thermal energy) is summarized

in Table 1. By the comparison between different energy modules in terms of energy distribution, it can be concluded that the integration of PV and T modules can synergistically improve the electrical and thermal performance of dual energy modules.

Table 1. Energy distribution of independent PV modules/T modules/PV/T modules.

Energy Distribution		Proportion of Total Energy (%)		
		PV	**T**	**PV/T**
Electricity		14.3	/	17.8
Heat energy	Water flow	/	18.7	21.6
	Heat pipe	/	31.4	/
Thermal energy	PV module	61.8	/	/
	T module	/	42.4	/
	PV/T module	/	/	36.6
Ambient thermal energy		17.2	20.8	18.9
Other energy losses		6.7	5.4	5.1

4. Conclusions

In this paper, we built a photovoltaic/thermal integrated pavement (PIPVT) geometry consisting of tempered glass panels, photovoltaic cells, serpentine copper tubes, and an ABS plastic base, which was simulated using COMSOL Multiphysics. Firstly, the energy distribution of solar, electrical, and thermal energy of the dual-energy module was simulated and explored. Then, the independent working characteristics and cooperative working characteristics of the PIPVT dual-energy module were compared. The results show the following:

(1) The solar energy utilization of a separate PV module is concentrated in the center of the tempered glass. The thermal T module was added, and the utilization rate of solar energy was also improved after circulating water was introduced. The working temperature of the module was also reduced, which is conducive to extending the life of the PV module.

(2) The simulation results show that the optimal operating voltage of the dual-energy module is 18 V and 1.66 A, which is in line with the expected results. The temperature drop value of the PIPVT module is consistent with the temperature increase value of the water flow in the serpentine copper tube, which reflects the heat collection effect of PIPVT and proves the important role of the heat T module.

(3) Only 14.3% of the electrical energy of the independent PV module is effectively utilized, while 18.7% of the thermal energy of the independent T module is utilized. The electric energy utilization rate of the dual-energy module is 17.8% and the thermal energy utilization rate is 21.6%.

While PV/T technology has improved solar energy efficiency, a comprehensive economic analysis of the system's financial performance is essential to identify cost-saving opportunities. Furthermore, the operational efficiency is influenced by various factors, such as weather conditions and maintenance practices. Therefore, conducting a further analysis of these factors is vital for optimizing system performance and guiding future improvements.

Author Contributions: B.Z.: Writing—Review and Editing, Supervision, Funding Acquisition, Project Administration; H.L.: Investigation, Data Curation, Writing—Original Draft; C.W.: Writing—Review and Editing; D.W.: Writing—Review and Editing; X.M.: Conceptualization, Supervision. All authors have read and agreed to the published version of the manuscript.

Funding: This work was supported by the Engineering Research Center of Ministry of Education of Transportation Materials, Chang'an University [300102313504].

Data Availability Statement: The raw data supporting the conclusions of this article will be made available by the authors on request.

Conflicts of Interest: The funders had no role in the design of the study; in the collection, analyses, or interpretation of data; in the writing of the manuscript; or in the decision to publish the results.

References

1. Attílio, L.A.; Faria, J.R.; Silva, E.C.D. Countervailing Impacts of Fossil Fuel Production and Exports of Electrical Goods on Energy Transitions and Climate Change. *J. Clean. Prod.* **2024**, *464*, 142797. [CrossRef]
2. Zhao, Y.; Sun, H.; Ma, D. Exploring the impact of carbon finance policy on photovoltaic market development–An experience from China. *Sol. Energy* **2024**, *272*, 112494. [CrossRef]
3. Jäger-Waldau, A. Snapshot of photovoltaics—May 2023. *EPJ Photovolt.* **2023**, *14*, 23. [CrossRef]
4. Gernaat, D.E.H.J.; de Boer, H.S.; Dammeier, L.C.; van Vuuren, D.P. The role of residential rooftop photovoltaic in long-term energy and climate scenarios. *Appl. Energy* **2020**, *279*, 115705. [CrossRef]
5. Verdugo, C.; Candela, J.I.; Luna, A.; Rodriguez, P. Power station for large scale photovoltaic power plants. In Proceedings of the 2017 IEEE 6th International Conference on Renewable Energy Research and Applications (ICRERA), San Diego, CA, USA, 5–8 November 2017; IEEE: Piscataway, NJ, USA, 2017; pp. 768–773.
6. Li, Z.; Ma, T.; Yang, H.; Lu, L.; Wang, R. Transparent and colored solar photovoltaics for building integration. *Sol. RRL* **2021**, *5*, 2000614. [CrossRef]
7. Kolokotroni, M.; Shittu, E.; Santos, T.; Ramowski, L.; Mollard, A.; Rowe, K.; Wilson, E.; Filho, J.P.d.B.; Novieto, D. Cool roofs: High tech low cost solution for energy efficiency and thermal comfort in low rise low income houses in high solar radiation countries. *Energy Build.* **2018**, *176*, 58–70. [CrossRef]
8. Rahmani-andebili, M. Canopying plug-in electric vehicles parking lots with photovoltaic panels. In Proceedings of the 2016 21st Conference on Electrical Power Distribution Networks Conference (EPDC), Karaj, Iran, 26–27 April 2016; IEEE: Piscataway, NJ, USA, 2016; pp. 1–4.
9. Energy, H.R. *Photovoltaic Noise Barriers*; Office of Natural Environment: Washington, DC, USA, 2017.
10. Kim, B.; Han, S.U.; Heo, J.; Jung, J. Proof-of-concept of a two-stage approach for selecting suitable slopes on a highway network for solar photovoltaic systems: A case study in South Korea. *Renew. Energy* **2020**, *151*, 366–377. [CrossRef]
11. Deshmukh, S.S.; Pearce, J.M. Electric vehicle charging potential from retail parking lot solar photovoltaic awnings. *Renew. Energy* **2021**, *169*, 608–617. [CrossRef]
12. Wang, H.; Jasim, A.; Chen, X. Energy harvesting technologies in roadway and bridge for different applications–A comprehensive review. *Appl. Energy* **2018**, *212*, 1083–1094. [CrossRef]
13. Lv, S.; Zhang, M.; Lai, Y.; Wu, Y.; Deng, J.; Guo, Y.; Feng, M.; Shi, G.; Zhang, B.; Ren, J.; et al. Comparative analysis of photovoltaic thermoelectric systems using different photovoltaic cells. *Appl. Therm. Eng.* **2023**, *235*, 121356. [CrossRef]
14. Abo-Zahhad, E.M.; Haridy, S.; Radwan, A.; El-Sharkawy, I.I.; Esmail, M.F. Thermal management of ultra high concentrator photovoltaic cells: Analysing the impact of sintered porous media microchannel heat sinks. *J. Clean. Prod.* **2024**, *465*, 142649. [CrossRef]
15. Bayrak, F.; Oztop, H.F. Effects of static and dynamic shading on thermodynamic and electrical performance for photovoltaic panels. *Appl. Therm. Eng.* **2020**, *169*, 114900. [CrossRef]
16. Singh, P.; Khanna, S.; Mudgal, V.; Newar, S.; Sharma, V.; Sundaram, S.; Reddy, K.; Mallick, T.K.; Becerra, V.; Hutchinson, D.; et al. Three dimensional analysis of dye-sensitized, perovskite and monocrystalline silicon solar photovoltaic cells under non uniform solar flux. *Appl. Therm. Eng.* **2021**, *182*, 115613. [CrossRef]
17. Johnsson, J.; Adl-Zarrabi, B. A numerical and experimental study of a pavement solar collector for the northern hemisphere. *Appl. Energy* **2020**, *260*, 114286. [CrossRef]
18. Farzan, H.; Zaim, E.H.; Ameri, M.; Amiri, T. Study on effects of wind velocity on thermal efficiency and heat dynamics of pavement solar collectors: An experimental and numerical study. *Renew. Energy* **2021**, *163*, 1718–1728. [CrossRef]
19. Ghalandari, T.; Baetens, R.; Verhaert, I.; Nasir, D.S.; Bergh, W.V.D.; Vuye, C. Thermal performance of a controllable pavement solar collector prototype with configuration flexibility. *Appl. Energy* **2022**, *313*, 118908. [CrossRef]
20. Yu, X.; Puppala, A.J.; Zhang, N. *Use of Geothermal Energy for Deicing Approach Pavement Slabs and Bridge Decks, Phase 1*; Department of Transportation, Research and Technology Implementation Office: Austin, TX, USA, 2017.
21. Mirzanamadi, R.; Hagentoft, C.E.; Johansson, P.; Johnsson, J. Anti-icing of road surfaces using hydronic heating pavement with low temperature. *Cold Reg. Sci. Technol.* **2018**, *145*, 106–118. [CrossRef]
22. Nasir, D.S.N.M.; Pantua, C.A.J.; Zhou, B.; Vital, B.; Calautit, J.; Hughes, B. Numerical analysis of an urban road pavement solar collector (U-RPSC) for heat island mitigation: Impact on the urban environment. *Renew. Energy* **2021**, *164*, 618–641. [CrossRef]
23. Pino, A.; Pino, F.J.; González, G.M.C.; Navas, S.J.; Guerra, J.; Cabello, G. PVT potential for a small-scale brewing process: A case study. *Therm. Sci. Eng. Prog.* **2024**, *53*, 102670. [CrossRef]
24. Yu, G.; Yang, H.; Yan, Z.; Ansah, M.K. A review of designs and performance of façade-based building integrated photovoltaic-thermal (BIPVT) systems. *Appl. Therm. Eng.* **2021**, *182*, 116081. [CrossRef]
25. Maghrabie, H.M.; Elsaid, K.; Sayed, E.T.; Abdelkareem, M.A.; Wilberforce, T.; Olabi, A. Building-integrated photovoltaic/thermal (BIPVT) systems: Applications and challenges. *Sustain. Energy Technol. Assess.* **2021**, *45*, 101151. [CrossRef]
26. Debbarma, M.; Sudhakar, K.; Baredar, P. Comparison of BIPV and BIPVT: A review. *Resour.-Effic. Technol.* **2017**, *3*, 263–271. [CrossRef]

27. Ren, H.; Quan, Z.; Wang, Z.; Wang, L.; Jing, H.; Zhao, Y. Performance simulation and analysis of a multi-energy complementary energy supply system for a novel BIPVT nearly zero energy building. *Energy Convers. Manag.* **2023**, *282*, 116879. [CrossRef]
28. Zhou, B.; Pei, J.; Nasir, D.M.; Zhang, J. A review on solar pavement and photovoltaic/thermal (PV/T) system. *Transp. Res. Part D Transp. Environ.* **2021**, *93*, 102753. [CrossRef]
29. Li, S.; Gu, W.; Liu, X.; Zhou, Y.; Chen, Z.; Zhang, X.; Ma, T. Pavement integrated photovoltaic thermal (PIPVT) system: A temporal and spatial analysis of energy and exergy performance. *J. Clean. Prod.* **2022**, *340*, 130782. [CrossRef]
30. Li, S.; Chen, Z.; Liu, X.; Zhang, X.; Zhou, Y.; Gu, W.; Ma, T. Numerical simulation of a novel pavement integrated photovoltaic thermal (PIPVT) module. *Appl. Energy* **2021**, *283*, 116287. [CrossRef]
31. Li, M.; Zhong, D.; Ma, T.; Kazemian, A.; Gu, W. Photovoltaic thermal module and solar thermal collector connected in series: Energy and exergy analysis. *Energy Convers. Manag.* **2020**, *206*, 112479. [CrossRef]
32. Chen, J.F.; Zhang, L.; Dai, Y.J. Performance analysis and multi-objective optimization of a hybrid photovoltaic/thermal collector for domestic hot water application. *Energy* **2018**, *143*, 500–516. [CrossRef]